



## Nodal and mixed finite elements for the numerical homogenization of 3D permeability

Anna Trykozko <sup>a</sup>, Wouter Zijl <sup>b</sup> and Alain Bossavit <sup>c</sup>

<sup>a</sup> *Institute of Environmental Engineering Systems, ul. Nowowiejska 20, 00-653 Warsaw, Poland, and Interdisciplinary Centre for Mathematical and Computational Modelling, ul. Pawińskiego 5a, 02-106 Warsaw, Poland*

E-mail: a.trykozko@icm.edu.pl

<sup>b</sup> *Netherlands Institute of Applied Geoscience TNO, P.O. Box 80015, 3508 TA Utrecht, The Netherlands*

E-mail: w.zijl@nitg.tno.nl

<sup>c</sup> *Électricité de France, 1 Avenue du Général-de-Gaulle, 92141 Clamart, France*

E-mail: alain.bossavit@der.edfgdf.fr

Received January 2000

The aim of upscaling is to determine equivalent homogeneous parameters at a coarse-scale from a spatially oscillating fine-scale parameter distribution. To be able to use a limited number of relatively large grid-blocks in numerical oil reservoir simulators or groundwater models, upscaling of the permeability is frequently applied. The spatial fine-scale permeability distribution is generally obtained from geological and geostatistical models. After upscaling, the coarse-scale permeabilities are incorporated in the relatively large grid-blocks of the numerical model. If the porous rock may be approximated as a periodic medium, upscaling can be performed by the method of homogenization. In this paper the homogenization is performed numerically, which gives rise to an approximation error. The complementarity between two different numerical methods – the conformal-nodal finite element method and the mixed-hybrid finite element method – has been used to quantify this error. These two methods yield respectively upper and lower bounds for the eigenvalues of the coarse-scale permeability tensor. Results of 3D numerical experiments are shown, both for the far field and around wells.

**Keywords:** bilateral bounds, complementarity, homogenization, mixed finite elements, nodal finite elements

### 1. Introduction

The basic idea of upscaling is to find a homogeneous permeability in such a way that the average behavior of the heterogeneous porous medium is conserved. The heterogeneous fine-scale permeability tensor may be strongly oscillating as a function of the fine-scale coordinates, but the coarse-scale permeability tensor obtained by upscaling is a smooth function of the coarse-scale coordinates.

The upscaled permeability may be considered as a kind of spatial average that relates the volume averaged quantities pressure, pressure gradient, flux and dissipation

in a similar way as the fine-scale relations between these quantities do. In other words, the upscaled permeability preserves the well-known forms of the fine-scale continuity equation, Darcy's law and dissipation equation on the coarse scale.

Arithmetic and harmonic averages are well known for flow respectively parallel and normal to layers. Equally well known is the geometric average for isotropic checkerboard configurations and for isotropic lognormal permeability distributions. Kirchhoff's method, in which Darcy's law is treated in the same way as Ohm's law applied to an electric network, is popular for more complex configurations. To avoid overly complex networks inherent to very large upscaling volumes, Kirchhoff's method is first applied to relatively small volumes and then the procedure is repeated to larger volumes containing the smaller volumes. In this reiterated form, the method is known under the name 'renormalization method' [16]. However, a disadvantage of this method is that directional effects in the form of off-diagonal coarse-scale permeability components cannot be represented.

To counter this disadvantage, the homogenization method, as originally developed in [5], has raised much interest [3,11,13,21,22,25]. For each upscaling cell this method requires the solution of three elliptic partial differential equations with periodic boundary conditions. Classical homogenization theory is based on multi-scale asymptotic expansions. However, in section 2 the results of homogenization will be summarized using 'preservation of equations' as guiding principle.

Boundary conditions that are consistent with the actual flow may be considered superior above – more or less arbitrary – periodic boundary conditions. However, this apparent superiority will be challenged. The coarse-scale permeability may be defined as the permeability that relates the gradient of the volume-averaged pressure to the volume-averaged flux. Alternatively, it may also be defined as the permeability that relates the gradient of the volume-averaged pressure to the volume-averaged dissipation. If the pressure gradient is periodic, these two definitions lead to the same coarse-scale permeability [31]. And if the two definitions may be applied simultaneously, both the coarse-scale Darcy's law and the coarse-scale dissipation equation are preserved in the same well-known form as they have on the fine scale. Not only preservation of Darcy's law, but also of the dissipation equation is important, because thermodynamic laws like Onsager's relations [9], are based on it.

Another advantage of periodic boundary conditions is that then error bounds of the numerical approximations can be rigorously established. The conformal-nodal finite element method is briefly summarized in section 3, while mixed-hybrid finite elements are introduced in section 4. A posteriori error bounds will be developed in section 5 following complementarity techniques [6,27], of which section 6 presents some numerical examples.

Finally, taking the 'real boundary conditions' into account means that not just the upscaling cell, but a much larger volume that includes the upscaling cell, has to be part of the computations. This is illustrated in section 7 for upscaling around a well.

There are many spatial scales in natural porous media. If the differences between the dimensions of the different heterogeneity scales are sufficiently large, application

of multi-scale asymptotic expansions shows that the different scales can be treated separately. Then homogenization can be applied to obtain medium-scale permeabilities from fine-scale permeabilities, while reiterated homogenization yields coarse-scale permeabilities from the medium-scale permeabilities, etc., just like in the renormalization technique [16]. However, scale separation is not always possible, for instance, if there are trends superimposed on the periodicity pattern. In such cases global upscaling may be considered as a more appropriate alternative. However, since there exist at least two equally justifiable global methods, yielding two different coarse-scale permeabilities, homogenization is still an acceptable alternative, as will be shown in section 7.

## 2. Homogenization

Let us consider the problem  $\operatorname{div} \mathbf{u} = 0$ ,  $\mathbf{u} = \mathbf{k} \cdot \mathbf{h}$ ,  $\operatorname{rot} \mathbf{h} = \mathbf{0}$  in a 3D domain  $D$  with nonhomogeneous boundary conditions. We assume topological triviality – a ‘contractible’ domain  $D$  – to avoid extraneous considerations. The tensor  $\mathbf{k} \in L^\infty(D)$  is symmetric and strictly positive and we will use the notation  $\mathbf{r}$  for the inverse of  $\mathbf{k}$ . This model has applications in many branches of physics [6]. Here,  $\mathbf{u}$  is the flux density multiplied by the dynamic viscosity (briefly the flux),  $\mathbf{h} = -\operatorname{grad} p$  is minus the gradient of the excess pressure (briefly the driving force) where the excess pressure  $p$  is the fluid pressure minus the hydrostatic pressure, and  $\mathbf{k}$  is the absolute permeability (briefly the permeability). Then  $\mathbf{u} = \mathbf{k} \cdot \mathbf{h}$  is Darcy’s law.

As has already been explained in the introduction,  $\mathbf{k}$  will generally vary on a ‘microscopic’ length scale, too fine to be included in numerical simulations, but has some ‘macroscopic’ homogeneity. In homogenization theory  $\mathbf{k}$  is assumed periodic, with a ‘periodicity cell’  $\Omega$  of much smaller size than  $D$ . By this we mean that there are three vectors  $\mathbf{d}_1, \mathbf{d}_2, \mathbf{d}_3$  such that  $\mathbf{k}(\mathbf{x} + \mathbf{d}_i) = \mathbf{k}(\mathbf{x})$  for all  $i$  and all points  $\mathbf{x}$  in  $D$ , except those too close to its boundary. The cell  $\Omega$  is than a parallelepiped built on the vectors  $\mathbf{d}_i$ .

Solving on  $\Omega$  what is called the ‘cell problem,’ to be presented below, provides a matrix  $\mathbf{K}$ , which expresses the macroscopic, or coarse-scale permeability of the homogenized medium. (One may want the coarse-scale permeability  $\mathbf{K}$  to take into account coarse-scale variations of  $\mathbf{k}$ . This way  $\mathbf{K}$  will depend on position within  $D$ . Take for  $\Omega$ , in that case, a box ‘anchored at’ the point of interest, with sides parallel to the vectors  $\mathbf{d}_i$ .)

Once  $\mathbf{K}$  has been obtained, one may solve instead of the original equations the much more manageable problem  $\operatorname{div} \mathbf{U} = 0$ ,  $\mathbf{U} = \mathbf{K} \cdot \mathbf{H}$ ,  $\operatorname{rot} \mathbf{H} = \mathbf{0}$  plus boundary conditions, where the fine-scale quantities  $\mathbf{u}, \mathbf{h}$  differ from the coarse-scale averages  $\mathbf{U}, \mathbf{H}$  by a locally periodic fine-scale fluctuation.

**The cell problem.** It consists in solving three similar elliptic flow problems for the quantities  $\mathbf{u}_i, \mathbf{h}_i = -\operatorname{grad} p_i, i = 1, 2, 3$ , on the periodicity cell  $\Omega$  with periodic boundary conditions for the three functions  $\chi_i = p_i + \mathbf{H}_i \cdot \mathbf{x}_i$ , where  $\mathbf{H}_i$  are three linearly independent constant vectors. For brevity in the expression of such periodicity conditions, we shall say that a function  $\chi$ , defined on  $\Omega$  and its boundary  $\Gamma = \partial\Omega$ , is ‘periodic

on  $\Gamma$  if  $\chi(\mathbf{x} + \mathbf{d}_i) = \chi(\mathbf{x})$  whenever both points  $\mathbf{x}$  and  $\mathbf{x} + \mathbf{d}_i$  belong to  $\Gamma$ . So, in the conventional formulation with the pressure as primary variable

$$\operatorname{div}(\mathbf{k} \cdot \operatorname{grad} p_i) = 0 \quad (\text{Boussinesq equation}), \quad (1.i)$$

in the ‘homogenization cell’  $\Omega$  and

$$\chi_i = p_i + \mathbf{H}_i \cdot \mathbf{x}_i \quad \text{periodic on } \Gamma \quad (\text{periodicity assumption}). \quad (1.ii)$$

The above equations represent three semi-definite problems, which have unique solutions  $p_i + c_i$  up to arbitrary constants  $c_i$ . The alternative ‘vector potential formulation’ will be introduced in section 5.

A convenient choice of  $\mathbf{H}_i$  is

$$H_{ij} = \delta_{ij} \quad (\text{component } j \text{ of } H - \text{vector } i), \quad (2)$$

yielding the orthonormal boundary conditions  $\chi_i = p_i + x_i$  is periodic on  $\Gamma$ . Then, based on the solutions of (1), the coarse-scale permeabilities are derived from the following formulas

$$K_{ij} = \langle \mathbf{k} \cdot \operatorname{grad} p_j \rangle_i = \left\langle \sum_{m=1}^3 k_{im} \frac{\partial p_j}{\partial x_m} \right\rangle \quad (\text{component } i \text{ of solution } j) \quad (3.i)$$

and/or

$$K_{ij} = \langle \operatorname{grad} p_i \cdot \mathbf{k} \cdot \operatorname{grad} p_j \rangle = \left\langle \sum_{m=1}^3 \sum_{n=1}^3 k_{mn} \frac{\partial p_i}{\partial x_n} \frac{\partial p_j}{\partial x_m} \right\rangle, \quad (3.ii)$$

where the brackets  $\langle \cdot \rangle$  denote volume averaging. Expression (3.i) represents ‘pressure-flux averaging’ to determine  $\mathbf{K}$  from the coarse-scale Darcy’s law  $\langle \mathbf{u}_i \rangle = -\mathbf{K} \cdot \operatorname{grad} \langle p_i \rangle$ , with  $-\partial \langle p_i \rangle / \partial x_j = \delta_{ij}$ . Expression (3.ii) corresponds to the coarse-scale dissipation equation and is a special case of ‘pressure-dissipation’ averaging [31].

Because of the periodic boundary conditions (1.ii), both pressure-flux averaging and pressure-dissipation averaging result in the same coarse-scale permeability tensor. However, the numerical algorithms differ, which may give rise to slight numerical differences. In cases without periodicity, the two averaging methods yield different results; this will be exemplified in section 7.

In the classical literature on homogenization, the above equations (1)–(3) are rigorously derived using dual-scale asymptotic expansions in which the fine-scale flow quantities are considered as depending on two sets of coordinates:

- (i) the fine-scale coordinates describing the permeability’s fine-scale oscillations, and
- (ii) the coarse-scale coordinates describing smooth coarse-scale variations [3,5,11,13, 21,22,25].

Here we have taken the much simpler approach to homogenization based on ‘physical insight’ involving the ‘principle of preservation of equations,’ as in [31].

### 3. The conformal nodal finite element method

The three elliptic problems (1) have to be solved numerically. To this end we introduce a simplicial mesh  $m$  of the homogenization cell  $\Omega$ , with congruence of boundary simplices by  $\mathbf{d}_i$  translation, which allows one to identify opposite nodes, edges and faces (thus turning  $\Omega$  into a topological 3-torus). Let  $\tilde{N}$ ,  $\tilde{E}$ ,  $\tilde{F}$ ,  $\tilde{T}$  stand for the sets of respectively nodes, edges, faces and tetrahedra, and  $N$ ,  $E$ ,  $F$ ,  $T$  for their numbers. The pressures  $p_i$  have to be approximated as piecewise linear. This is equivalent with determining the approximate solution using the well-known conformal-nodal (CN) finite element method with  $N$  piecewise linear basis functions  $\varphi_n(x_1, x_2, x_3)$ ,  $n = 1, 2, \dots, N$ .

The three approximate solutions  $p_i^{\text{CN}}(x_1, x_2, x_3)$ ,  $i = 1, 2, 3$ , are written as the linear combination

$$p_i^{\text{CN}}(x_1, x_2, x_3) = \sum_{n=1}^N p_{in} \varphi_n(x_1, x_2, x_3), \quad (4)$$

where  $p_{in}$ ,  $n = 1, 2, \dots, N$ , are the approximate node-based pressures for the three problems  $i = 1, 2, 3$ . Using the basis functions as test functions (Galerkin's method) and substituting (4) into the weak form of equations (1),

$$\int_{\Omega} \text{grad } \varphi_n \cdot \mathbf{k} \cdot \text{grad } p_i \, d\Omega = - \int_{\Gamma} \varphi_n \mathbf{u}_i \cdot \mathbf{v} \, d\Gamma$$

( $\mathbf{v}$  is the normal unit vector pointing out of the closed boundary  $\Gamma$ ), yields the following system of  $N$  linear equations for the  $N$  unknowns  $p_{in}$

$$\sum_{n=1}^N \left( \int_{\Omega} \text{grad } \varphi_m \cdot \mathbf{k} \cdot \text{grad } \varphi_n \, d\Omega \right) p_{in} = - \int_{\Gamma} \varphi_m \mathbf{u}_i \cdot \mathbf{v} \, d\Gamma, \quad m = 1, 2, \dots, N. \quad (5)$$

Each of the three systems (5) has an  $N \times N$  system matrix that is sparse, symmetric and positive semi-definite with a one-dimensional null-space. The systems have been solved using the preconditioned conjugate gradient method, with a preconditioner based on incomplete Cholesky decomposition [14,18].

**Numerical example 1** (Preferential flow paths). Let us consider the permeability pattern shown in figure 1. It represents an idealized version of a fissured porous medium. The intact rock has a permeability of 1 mD, while the high-permeable fissures have a permeability of 100 mD. There are no permeability variations in the  $y$  direction. The size of the homogenization cell is  $\Delta x \times \Delta y \times \Delta z = 0.8 \text{ m} \times 0.6 \text{ m} \times 1.2 \text{ m}$ . Counting equivalent nodes on two opposite boundaries of the homogenization cell only once, we obtain the number of active nodes  $N_a$ .

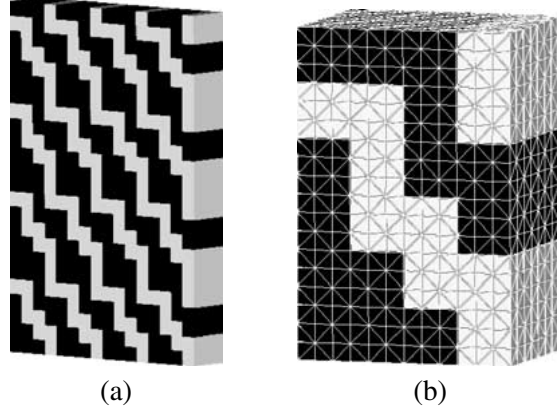


Figure 1. Idealized fissured medium (a) with finite element mesh (b); black blocks correspond to 1 mD and white ones to 100 mD. The right picture shows a coarse mesh with  $12 \times 8 \times 18$  active nodes.

Homogenization using the conformal-nodal finite element method performed on a finer mesh than the mesh shown in figure 1 with  $N_a = 20 \times 12 \times 30$ , yields the following approximate solutions

$$K_{ij}^{\text{CN}} = \begin{pmatrix} 10.83 & 0 & -12.69 \\ 0 & 42.25 & 0 \\ -12.69 & 0 & 21.60 \end{pmatrix} \text{mD}, \quad K_{\eta\mu}^{\text{CN}} = \begin{pmatrix} 30.00 & 0 & 0 \\ 0 & 42.25 & 0 \\ 0 & 0 & 2.430 \end{pmatrix} \text{mD},$$

where  $K_{\eta\mu}^{\text{CN}}$  represents the coarse-scale permeability components in the principal  $\eta\mu$  coordinate system of the matrix  $K_{ij}^{\text{CN}}$ , which is obtained by a rotation of  $-56.50^\circ$  with respect to the original  $(x, z)$  coordinate system (note that  $\arctan(\Delta z/\Delta x) = -56.31^\circ$ ). We observe that  $K_{22}^{\text{CN}} = 42.25$  mD is the arithmetic average, as it should be.

To study the accuracy of the approximate solution, computations were performed for a sequence of uniformly refined meshes. Denoting the eigenvalues  $K_{\eta\eta}^{\text{CN}}$  as  $\Lambda_\eta^{\text{CN}}$ , figures 2 and 3 show the rate of convergence. As the mesh is becoming finer, the final results seem to approach an asymptote. To assess the quality of the approximate solution, the mixed-hybrid finite element method will be introduced in the next section.

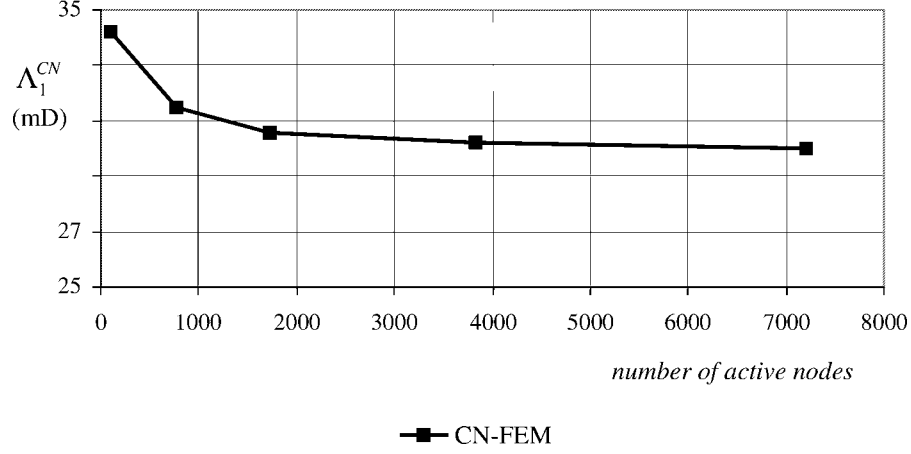
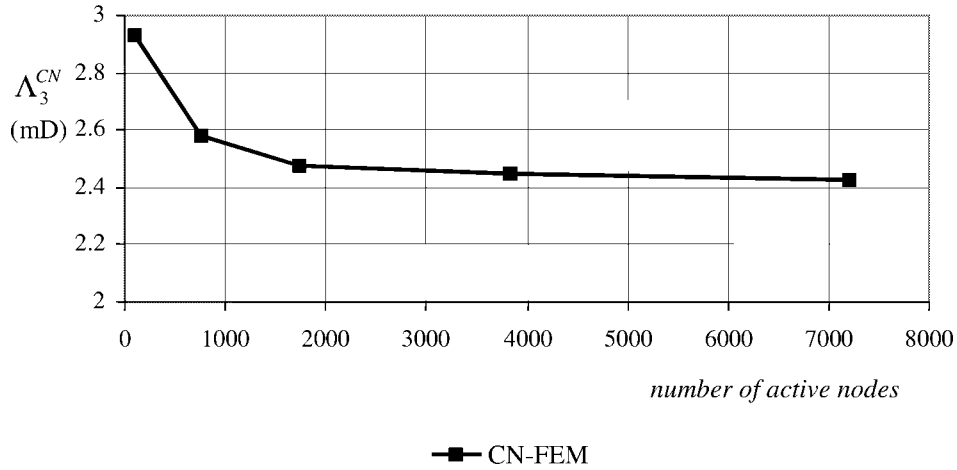
#### 4. The mixed finite element method and hybridization

Let us rewrite the cell problem (1) in the following, theoretically equivalent form, which emphasizes the role of the fluxes  $\mathbf{u}_i$ ,  $i = 1, 2, 3$ :

$$\operatorname{div} \mathbf{u}_i = 0 \quad \text{in } \Omega \quad (\text{continuity equation}), \quad (6.i)$$

$$\operatorname{grad} p_i = -\mathbf{r} \cdot \mathbf{u}_i \quad \text{in } \Omega \quad (\text{Darcy's law}), \quad (6.ii)$$

$$\chi_i = \mathbf{u}_i - \mathbf{U}_i \quad \text{is periodic on } \Gamma, \quad (6.iii)$$

Figure 2. Eigenvalue  $\Lambda_1^{CN}$  of coarse-scale permeability.Figure 3. Eigenvalue  $\Lambda_3^{CN}$  of coarse-scale permeability.

where  $U_i$  represent three linearly independent constant vectors and  $\langle \chi_i \rangle = \mathbf{0}$ . If we choose the orthonormal conditions  $U_{ij} = -\delta_{ij}$  (component  $j$  of  $U$ -vector  $i$ ), the coarse-scale resistivities are given as

$$R_{ij} = \langle \mathbf{r} \cdot \mathbf{u}_j \rangle_i = \left\langle \sum_{m=1}^3 r_{im} u_{jm} \right\rangle \quad (\text{pressure-flux averaging}), \quad (7.i)$$

and

$$R_{ij} = \langle \mathbf{u}_i \cdot \mathbf{r} \cdot \mathbf{u}_j \rangle = \left\langle \sum_{m=1}^3 \sum_{n=1}^3 r_{mn} u_{in} u_{jm} \right\rangle \quad (\text{flux-dissipation averaging}). \quad (7.ii)$$

Of course, the orthonormal boundary condition (1.ii) and (2) combined with expressions (3) are also a form of boundary condition (6.iii), finally leading to the same coarse-scale permeability.

Using the same simplicial mesh as in section 3, we now assign one degree of freedom for  $\mathbf{u}_i \cdot \mathbf{v}$  to each face  $f \in \tilde{F}$ , denoted by  $u_{if}$ . The solution of (6) is approximated using affine mixed finite elements. Here the lowest order Raviart–Thomas space [20,23] is used as approximation space for the flux. The space for the pressure is a multiplier space. Let us recall that  $F$  is the number of faces and  $T$  is the number of tetrahedra.

The mixed approximation (MA) to the flux is

$$\mathbf{u}_i^{\text{MA}}(x_1, x_2, x_3) = \sum_{f=1}^F u_{if} \boldsymbol{\phi}_f(x_1, x_2, x_3), \quad (8)$$

where the basis functions  $\boldsymbol{\phi}_f(x_1, x_2, x_3)$ , piecewise linear, vector valued, are defined such that the continuity requirements for  $\boldsymbol{\phi}_f \cdot \mathbf{v}_f$  on each face  $f = 1, 2, \dots, F$  are satisfied ( $\mathbf{v}_f$  is the normal unit vector on face  $f$  pointing out of the tetrahedron under consideration. Then  $u_{if}$ ,  $f = 1, 2, \dots, F$ , are the approximate flux components normal to the faces). Note that the continuity equation (6.i) is exactly satisfied with this kind of approximation (cf. [15]).

The mixed approximation to the pressure is

$$p_i^{\text{MA}}(x_1, x_2, x_3) = \sum_{t=1}^T p_{it} \varphi_t(x_1, x_2, x_3), \quad (9)$$

where the  $\varphi_t(x_1, x_2, x_3)$ ,  $t = 1, 2, \dots, T$ , are piecewise constant scalar functions. Then  $p_{it}$ ,  $t = 1, 2, \dots, T$ , are the approximate tetrahedral pressures.

Using the basis functions as test functions and substituting approximations (8) and (9) into the complementary weak form of equations (6),

$$\int_{\Omega} (\boldsymbol{\phi}_f \cdot \mathbf{r} \cdot \mathbf{u}_i - p_i \operatorname{div} \boldsymbol{\phi}_f) \, d\Omega = - \int_{\Gamma} p_i \boldsymbol{\phi}_f \cdot \mathbf{v} \, d\Gamma, \quad \operatorname{div} \mathbf{u}_i = 0,$$

yields the following  $F + T$  equations for the  $F + T$  unknowns  $u_{if}$  and  $p_{it}$ :

$$\sum_{m=1}^F \left( \int_{\Omega} \boldsymbol{\phi}_f \cdot \mathbf{r} \cdot \boldsymbol{\phi}_m \, d\Omega \right) u_{im} - \sum_{t=1}^T \left( \int_{\Omega} \varphi_t \operatorname{div} \boldsymbol{\phi}_f \, d\Omega \right) p_{it} = - \int_{\Gamma} p_i \boldsymbol{\phi}_f \cdot \mathbf{v} \, d\Gamma,$$

$$f = 1, 2, \dots, F, \quad (10.i)$$

$$- \sum_{f=1}^F \left( \int_{\Omega} \varphi_t \operatorname{div} \boldsymbol{\phi}_f \, d\Omega \right) u_{if} = 0, \quad t = 1, 2, \dots, T. \quad (10.ii)$$

The mixed formulation (10) requires the solution of a ‘saddle point problem,’ i.e., a linear system in which the large  $(F + T) \times (F + T)$  system matrix is not positive

definite, which can be very expensive to solve. The advantages of using the computationally much more efficient node-based finite element method has challenged some researchers to use it also for solving the complementary problem (the problem in which  $\mathbf{r}$  occurs instead of  $\mathbf{k}$ ). For perfectly layered media, i.e., for media in which the permeability is a scalar depending on only one coordinate, say the  $x_3$ -coordinate, the simple complementary equation  $\text{div}(r \text{ grad } u_3) = 0$  holds, together with the primary equations  $\text{div}(k \text{ grad } h_i) = 0$ ,  $i = 1, 2$ . Hence, only three uncoupled, sparse, symmetric and positive definite  $N \times N$  system matrices have to be solved. Layered media have many practical applications in earth science [30]. However, extension to general heterogeneous media requires  $\mathbf{k}(\mathbf{x}) \in C^{(1)}(\Omega)$ , which makes this approach irrelevant for homogenization.

Fortunately, another alternative approach brings relief: the hybrid form of equations (10), as introduced in [2] (see also [7]). The hybrid method is based on the domain decomposition technique: the  $F$  continuity requirements for the normal fluxes  $u_{if} = \mathbf{u}_{if} \cdot \mathbf{v}_f$  at the faces are first relaxed, leading to  $2F$  unknown normal fluxes  $\alpha_{if+}$  and  $\alpha_{if-}$  per face. Then the continuity is reintroduced by  $F$  Lagrange multipliers  $\gamma_{if}$ ,  $f = 1, 2, \dots, F$ . It can be proved that the hybrid form of the mixed finite element method is algebraically equivalent to the mixed finite element method, however, with a different resulting system of linear equations:

$$\begin{pmatrix} A & B & C \\ B^T & 0 & 0 \\ C^T & 0 & 0 \end{pmatrix} \begin{pmatrix} \alpha_i \\ \beta_i \\ \gamma_i \end{pmatrix} = \begin{pmatrix} D_{i1} \\ D_{i2} \\ D_{i3} \end{pmatrix}. \quad (11)$$

The  $2F$  unknown normal fluxes  $\alpha_i$  can be eliminated in terms of the  $T$  pressures  $\beta_i$  and the  $F$  Lagrange multipliers  $\gamma_i$ . Moreover, it turns out that the pressures can easily be eliminated in terms of the Lagrange multipliers alone. In this way the solution of the following much simpler sparse, symmetric and strictly positive definite linear system has to be computed

$$M\gamma_i = Z_i, \quad (12.i)$$

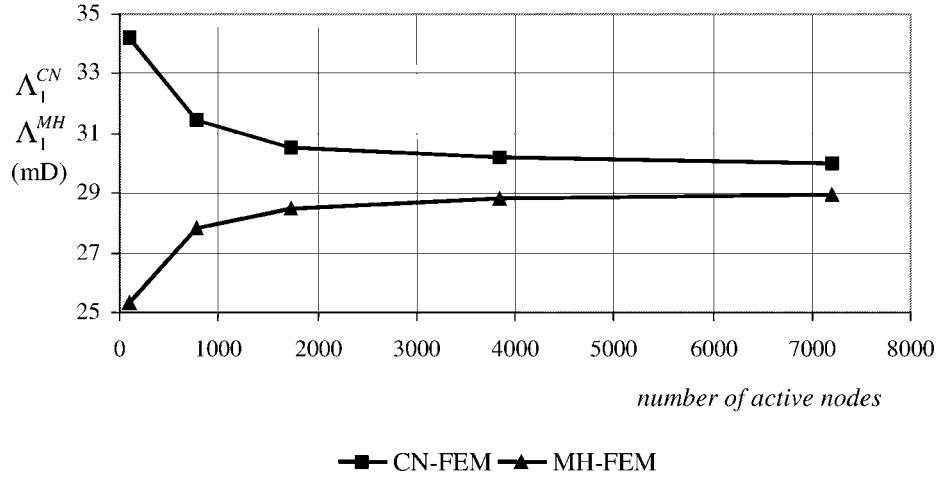
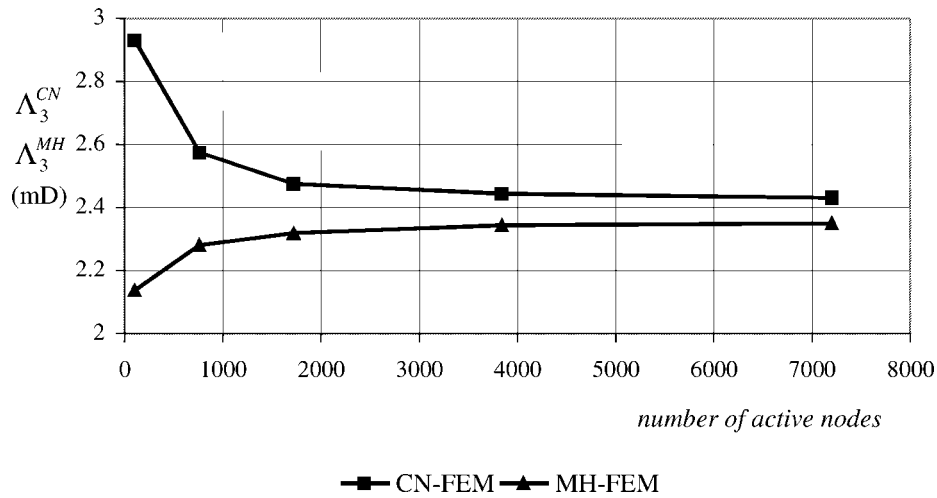
where

$$M = C^T(A^{-1} - A^{-1}B(B^T A^{-1}B)^{-1}B^T A^{-1})C \quad (12.ii)$$

and

$$Z_i = C^T A^{-1}(D_{i1} - B(B^T A^{-1}B)^{-1}(B^T A^{-1}D_{i1} - D_{i2})) - D_{i3}. \quad (12.iii)$$

The submatrices of  $M$  and the subcolumns of  $Z_i$  can be derived independently for every tetrahedral element and are then incorporated in respectively the global system matrix and the right-hand side columns. The approximation spaces of (8) have one unknown Lagrange multiplier per face, hence the resulting linear system (12) has an  $F \times F$  system matrix that is sparse, symmetric and positive definite with a one-dimensional null-space. Equation (12.i) is solved using the preconditioned conjugate gradient method, with a preconditioner based on incomplete Cholesky decomposition [14,18].

Figure 4. Eigenvalues  $\Lambda_1^{CN}$  and  $\Lambda_1^{MH}$  of coarse-scale permeability.Figure 5. Eigenvalues  $\Lambda_3^{CN}$  and  $\Lambda_3^{MH}$  of coarse-scale permeability.

Because of the periodic boundary conditions the actual sizes of the resulting linear systems are smaller since equivalent nodes, edges and faces on two opposite boundaries of the homogenization cell are counted only once.

The mesh has been constructed by first generating  $N_a$  hexahedra, which means that the number of *active* nodes is  $N_a$ . Then dividing the hexahedra into five tetrahedra yields  $T = 5N_a$  tetrahedra, each tetrahedron having four faces shared by two, yielding a number of  $F_a = 10N_a$  active faces. From the Euler–Poincaré formula it follows that the number of active edges  $E_a = 6N_a + 1$ . Since the conformal nodal and mixed hybrid method yield matrices with comparable sparseness, this means that system (12) is one order of magnitude greater than system (5) obtained by the conformal nodal finite

element method. The algebraically equivalent edge-based finite element method for the vector potential yields a smaller  $E \times E$  system, but its matrix is less sparse [6]. Whether edge elements can compete with mixed-hybrid elements will be the subject of a forthcoming paper. Here the computational disadvantage of the mixed hybrid method with respect to the conformal nodal method is accepted in order to estimate a posteriori error bounds: mixed elements and edge elements have ‘lower bound properties’ that complement the ‘upper bound properties’ of nodal elements. Before giving the proof, this will be illustrated in a numerical example.

**Numerical example 1** (Preferential flow paths using mixed-hybrid FEM). Using the same problem and mesh as in the example of section 3, the mixed-hybrid (MH) finite element method yields

$$K_{ij}^{\text{MH}} = \begin{pmatrix} 10.46 & 0 & -12.26 \\ 0 & 42.25 & 0 \\ -12.26 & 0 & 20.87 \end{pmatrix} \text{ mD},$$

$$K_{\eta\mu}^{\text{MH}} = \begin{pmatrix} 28.98 & 0 & 0 \\ 0 & 42.25 & 0 \\ 0 & 0 & 2.352 \end{pmatrix} \text{ mD}.$$

Again, the computations were repeated for a sequence of uniformly refined meshes. Figures 4 and 5 suggest that the conformal-nodal finite element method yields upper bounds of the eigenvalues of the homogenized permeability, while the mixed-hybrid finite element method yields lower bounds. Numerical 2D experiments performed by [24] have also lead to the suggestion of bilateral error bounds. That error bounds are really the case will be proved in section 5.

## 5. Upper and lower bounds

Below, a proof of the bilateral upper/lower bound properties will be based on complementarity techniques [6,27] and on the characterization of eigenvalues by the inf–sup condition for the Rayleigh quotient.

*Pressure-dissipation averaging combined with conformal-nodal finite elements.* For symmetric and strictly positive definite fine-scale permeability tensors, solving equations (1.i), (1.ii) is equivalent with minimizing the strictly positive definite functional  $\Theta(\theta) = \langle \text{grad } \theta \cdot \mathbf{k} \cdot \text{grad } \theta \rangle > 0$  over functions  $\theta$  subject to the periodicity condition (1.ii), i.e.,  $\theta_i + \mathbf{H}_i \cdot \mathbf{x}_i$  periodic on  $\Gamma$ .

If the coarse-scale permeability tensor is defined by pressure-dissipation averaging (by  $\text{grad}\langle p_i \rangle \cdot \mathbf{K} \cdot \text{grad}\langle p_j \rangle = \langle \text{grad } p_i \cdot \mathbf{k} \cdot \text{grad } p_j \rangle$ ), we find  $\text{grad}\langle p_i \rangle \cdot \mathbf{K} \cdot \text{grad}\langle p_i \rangle = \Theta(p_i)$ . The orthonormal boundary conditions (2) yield  $\text{grad}\langle p_i \rangle \cdot \mathbf{K} \cdot \text{grad}\langle p_j \rangle = K_{ij}$ . Hence,  $0 < K_{ii} = \Theta(p_i) \leq \Theta(\theta_i)$ .

The linear system (5), here obtained by the Galerkin method, can also be obtained by the Ritz method [26], which is based on the principle of least action to find nodal pressures that minimize the dissipation. Therefore, solving equations (5) corresponds to the above-presented minimization method. However, in this case the piecewise linear approximations  $p_i^{\text{CN}}(\mathbf{x})$  belong to a function space that is a finite-dimensional subspace of the function space for the exact solution  $p_i(\mathbf{x})$ . Because  $\Theta(p_i^{\text{CN}}) \geq \Theta(p_i) > 0$ , the exact minimum cannot be found in the subspace, except for cases where the exact solution is piecewise linear. In other words, for any arbitrary driving force  $\mathbf{H} = -\text{grad } P$  with unit magnitude  $|\mathbf{H}| = 1$ , the approximate dissipation is greater than or equal to the exact dissipation

$$\mathbf{H} \cdot \mathbf{K}^{\text{CN}} \cdot \mathbf{H} \geq \mathbf{H} \cdot \mathbf{K} \cdot \mathbf{H} > 0, \quad \mathbf{H} \cdot \mathbf{H} = 1. \quad (13)$$

The left-hand and right-hand sides of (13) are just the Rayleigh quotient characterization of the eigenvalues of respectively  $\mathbf{K}^{\text{CN}}$  and  $\mathbf{K}$ . We shall use this to prove that the approximate eigenvalues  $\Lambda_1^{\text{CN}}, \Lambda_2^{\text{CN}}, \Lambda_3^{\text{CN}}$  are greater than or equal to the exact eigenvalues  $\Lambda_1, \Lambda_2, \Lambda_3$ .

*Eigenvalues as error estimates.* First we introduce some mathematical preliminaries.

If  $f$  is a real-valued function on a set  $X$ , we denote by  $\inf(f)$  its greatest lower bound and by  $\sup(f)$  its smallest upper bound:  $\inf(f) = \inf\{f(x): x \in X\}$ , where the right-hand side is understood as ‘greatest lower bound of the braced family of real numbers’. A similar definition holds for  $\sup(f)$ . If the bounds do not exist, we make them exist in all cases by the usual trick of adding  $\pm\infty$  to the real line.

**Lemma 1.** If  $g(x) \geq f(x)$  for all  $x$  in  $X$ , then  $\inf(g) \geq \inf(f)$  and  $\sup(g) \geq \sup(f)$ .

*Proof.* By definition  $f(x) \geq \inf(f) \forall x$ , hence  $g(x) \geq \inf(f) \forall x$  by transitivity of  $\geq$ . So  $\inf(f)$  is a lower bound to  $g$ , hence smaller than the greatest one  $\inf(g)$ , therefore  $\inf(f) \leq \inf(g)$ .  $\square$

Next, let  $\mathfrak{N}$  be a family of subsets of  $X$ , and let a real-valued function  $f$  of  $A \in \mathfrak{N}$  be given. Set  $\inf_A \sup_x(f) = \inf\{\sup\{f(x): x \in A\}, A \in \mathfrak{N}\}$ , and the same for  $\sup_A \inf_x(f)$ .

**Lemma 2.** If  $g(x) \geq f(x)$  for all  $x$  in  $X$ , then  $\inf_A \sup_x(g) \geq \inf_A \sup_x(f)$ .

*Proof.* If  $g(x) \geq f(x)$  for all  $x \in X$ , and hence for all  $x \in A$ , then  $\sup\{g(x): x \in A\} \geq \sup\{f(x): x \in A\}$  by lemma 1, hence two functions defined on  $\mathfrak{N}$ , to which the lemma is applied again.  $\square$

Now let us recall the Rayleigh quotient characterization of eigenvalues. For a symmetric positive definite matrix  $\mathbf{M}$  of dimension  $n$ , the  $\eta$ th eigenvalue (each of them being counted with its multiplicity, and labeled in nondescending order), is [10,28]

$$\lambda_\eta(\mathbf{M}) = \inf \left\{ \sup \left\{ \frac{\mathbf{x} \cdot \mathbf{M} \cdot \mathbf{x}}{\mathbf{x} \cdot \mathbf{x}} : \mathbf{x} \in Y - \{0\} \right\} : Y \right\}, \quad (14.i)$$

where  $Y$  spans the set of  $\eta$ -dimensional subspaces of  $X$ . Alternatively,

$$\lambda_{n-\eta+1}(\mathbf{M}) = \sup \left\{ \inf \left\{ \frac{\mathbf{x} \cdot \mathbf{M} \cdot \mathbf{x}}{\mathbf{x} \cdot \mathbf{x}} : \mathbf{x} \in Y - \{0\} \right\} : \dim(Y) = \eta \right\}. \quad (14.ii)$$

**Proposition.** If  $\mathbf{x} \cdot \widehat{\mathbf{M}} \cdot \mathbf{x} \geq \mathbf{x} \cdot \mathbf{M} \cdot \mathbf{x}$  for all  $\mathbf{x} \in X$ , then  $\lambda_\eta(\widehat{\mathbf{M}}) \geq \lambda_\eta(\mathbf{M})$  for all  $\eta$ .

*Proof.* Apply lemma 2 to  $f(\mathbf{x}) = (\mathbf{x} \cdot \mathbf{M} \cdot \mathbf{x})/(\mathbf{x} \cdot \mathbf{x})$  and  $g(\mathbf{x}) = (\mathbf{x} \cdot \widehat{\mathbf{M}} \cdot \mathbf{x})/(\mathbf{x} \cdot \mathbf{x})$ . Sets  $A$  are the  $\eta$ -dimensional subspaces minus the origin.  $\square$

Having finished the expose of mathematical preliminaries, we go back to equation (13). Matrices  $\mathbf{M}$  and  $\widehat{\mathbf{M}}$  are now identified with  $\mathbf{K}$  and  $\mathbf{K}^{\text{CN}}$ , respectively, and  $X$  has three dimensions. We then find that  $\Lambda_\eta^{\text{CN}} = \lambda_\eta(\mathbf{K}^{\text{CN}}) \geq \lambda_\eta(\mathbf{K}) = \Lambda_\eta$  for all  $\eta = 1, 2, 3$ . In other words, the three approximate eigenvalues of the coarse-scale permeability tensor are upper bounds, as was asserted without proof in an earlier paper [31]. One may feel surprised by this result, in view of the well-known fact that eigenvalues of a symmetric positive operator, in an infinite dimensional Hilbert space, are *not* systematically bounded by those of its matrix approximation, except for the lowest one [10]. However, the situation here is different, because the operators that are compared act on the *same* vector space  $X$ .

*Flux-dissipation averaging combined with mixed-hybrid finite elements.* Let us now derive lower bounds. These can be found in an almost similar way by solving the complementary problem. Since  $\mathbf{u}$  is solenoidal (see (6.i)), it can be expressed by a vector potential  $\boldsymbol{\psi}$  such that  $\mathbf{u} = \text{rot } \boldsymbol{\psi}$ . Moreover, since  $\text{grad } p$  is irrotational, it follows from (6.ii) that  $\text{rot}(\mathbf{r} \cdot \mathbf{u}) = \mathbf{0}$ . Hence the vector potential satisfies the equation  $\text{rot}(\mathbf{r} \cdot \text{rot } \boldsymbol{\psi}) = \mathbf{0}$  (cf. [19]), which is an alternative for the well-known pressure equation  $\text{div}(\mathbf{k} \cdot \text{grad } p) = 0$  [6,27]. Again, solving the complementary equation is equivalent to minimizing the dissipation functional  $\Xi(\boldsymbol{\xi}) = \langle \text{rot } \boldsymbol{\xi} \cdot \mathbf{r} \cdot \text{rot } \boldsymbol{\xi} \rangle$  for all functions  $\boldsymbol{\xi}(\mathbf{x})$  satisfying a periodicity boundary condition analogous to (6.ii), namely  $\boldsymbol{\chi}_i = \boldsymbol{\psi}_i(\mathbf{x}) - \frac{1}{2} \mathbf{U}_i \times \mathbf{x}$  is periodic on  $\Gamma$ , for a given three-component vector  $\mathbf{U}_i$ .

Defining the coarse-scale resistivity tensor  $\mathbf{R}$  by flux-dissipation averaging, i.e., by  $\langle \mathbf{u}_i \rangle \cdot \mathbf{R} \cdot \langle \mathbf{u}_j \rangle = \langle \mathbf{u}_i \cdot \mathbf{r} \cdot \mathbf{u}_j \rangle$ , yields  $\langle \mathbf{u}_i \rangle \cdot \mathbf{R} \cdot \langle \mathbf{u}_i \rangle = \Xi(\boldsymbol{\psi}_i) \leq \Xi(\boldsymbol{\xi}_i)$ . (For periodic media,  $\mathbf{R}$  is the inverse of the pressure-dissipation permeability tensor introduced in the first subsection, as detailed in [31].) However, in the next subsection the relationship will be established.) Since the flux is periodic the vector functions  $\boldsymbol{\chi}_i = \boldsymbol{\psi}_i(\mathbf{x}) - \frac{1}{2} \mathbf{U}_i \times \mathbf{x}$ , where  $\mathbf{U}_i = \langle \mathbf{u}_i \rangle = \text{rot} \langle \boldsymbol{\psi}_i \rangle$ , are periodic too. The orthonormal boundary condition for the vector potential is:  $\chi_{ij} = \psi_{ij} - \frac{1}{2} \varepsilon_{ijk} x_k$  is periodic on  $\Gamma$ . ( $\varepsilon_{123} = \varepsilon_{231} = \varepsilon_{312} = 1$ ,  $\varepsilon_{321} =$

$\varepsilon_{213} = \varepsilon_{132} = -1$ ,  $\varepsilon_{ijk} = 0$  otherwise.) This condition yields  $\langle \psi_{ij} \rangle = \frac{1}{2} \varepsilon_{ijk} x_k + \langle \chi_{ij} \rangle$ , with constant  $\langle \chi_{ij} \rangle$ , from which it follows that  $U_{ij} = -\delta_{ij}$ . Hence, the simple expression  $0 < R_{ii} = \Xi(\boldsymbol{\psi}_i) \leq \Xi(\boldsymbol{\xi}_i)$  holds, from which it follows that also the three eigenvalues  $T_\eta$  of  $\mathbf{R}$  are minimal.

The linear system (11) yields approximate solutions  $\mathbf{u}_i^{\text{MH}}$  and  $p_i^{\text{MH}}$  of (6). In this solution process the continuity requirements are satisfied as part of the computational procedure, which renders (11) equivalent to (10). Moreover, the computational procedure is such that the divergence terms in (10) are forced to be equal to zero. Hence, solution  $\alpha$  satisfies equations (10) and (11) in the simplified form  $A\alpha = D_1$ . We will now show that the thus-obtained solution  $\alpha$  minimizes  $\mathbf{U} \cdot \mathbf{R} \cdot \mathbf{U}$  for any choice of  $\mathbf{U}$ .

If the equation for the vector potential  $\text{rot}(\mathbf{r} \cdot \text{rot} \boldsymbol{\psi}) = \mathbf{0}$  is satisfied, the irrotational vector  $\mathbf{r} \cdot \text{rot} \boldsymbol{\psi}$  may be written as  $-\text{grad } p$ . Then it follows from the vector identity  $\text{div}(\mathbf{u} \times \mathbf{v}) = -\mathbf{u} \cdot \text{rot} \mathbf{v} + \mathbf{v} \cdot \text{rot} \mathbf{u}$  that  $(\text{rot} \boldsymbol{\varepsilon}) \cdot \mathbf{r} \cdot (\text{rot} \boldsymbol{\psi}) = -\text{div}(\boldsymbol{\varepsilon} \times \text{grad } p)$ . Let us now interpret  $\boldsymbol{\varepsilon}$  as a test function. In the Galerkin approach applied to the complementary formulation, the test functions  $\text{rot} \boldsymbol{\varepsilon}$  are chosen equal to the interpolation functions  $\boldsymbol{\phi}_f$ . As a consequence, defining  $\mathbf{u} = \text{rot} \boldsymbol{\psi}$  and using the vector identity  $\text{div}(\boldsymbol{\varepsilon} \times \text{grad } p) = \text{grad } p \cdot \text{rot} \boldsymbol{\varepsilon}$ , the expression  $\boldsymbol{\phi}_f \cdot \mathbf{k}^{-1} \cdot \mathbf{u} - p \text{div} \boldsymbol{\phi}_f = -\text{div}(p \boldsymbol{\phi}_f)$  is found. Integration over the homogenization cell and using Gauss' integral theorem yields the complementary weak form given in section 4. Taking into account that  $\text{div} \boldsymbol{\phi}_f = 0$ , and substituting approximation (8) for  $\mathbf{u}$  into the complementary weak form, yields the linear system (10.i) in which the divergence term is dropped, i.e.,  $A\alpha = D_1$ . This proves that the mixed hybrid formulation (11) is algebraically equivalent with solving the equation for the vector potential formulation.

For the 'classical' conformal nodal method it is well known that the Galerkin method is equivalent with the Ritz method, which is based on minimization of the dissipation functional [26]. In a similar way, also the Galerkin-type mixed-hybrid method is equivalent with Ritz minimization, which proves that the mixed hybrid formulation (11) minimizes  $\mathbf{U} \cdot \mathbf{R} \cdot \mathbf{U}$  for any choice of  $\mathbf{U}$ .

Again, the piecewise linear approximation space for the flux yields an approximation space for  $\mathbf{u}_i^{\text{MH}}(\mathbf{x})$  which is a subspace of the function space of the exact solution. Therefore, since  $\Xi(\mathbf{u}_i^{\text{MH}}) \geq \Xi(\mathbf{u}_i) > 0$ , the exact minimum cannot be reached, except if the exact solution  $\mathbf{u}_i$  is piecewise linear. As a result, for any arbitrary unit flux field  $\mathbf{U}$ ,  $|\mathbf{U}| = 1$ , the approximate dissipation is greater than or equal to the exact dissipation, i.e.,

$$\mathbf{U} \cdot \mathbf{R}^{\text{MH}} \cdot \mathbf{U} \geq \mathbf{U} \cdot \mathbf{R} \cdot \mathbf{U} > 0, \quad (15)$$

where  $\mathbf{R}^{\text{MH}}$  and  $\mathbf{R}$  denote respectively the mixed-hybrid approximation and the exact value of the homogenized resistivity tensor. This means that the eigenvalues of  $\mathbf{R}^{\text{MH}} - \mathbf{R}$  are non-negative and, hence,  $R_{ii}^{\text{MH}} \geq R_{ii}$ . In the same way as for the conformal-nodal method, this property yields the error bounds  $\lambda_\eta(\mathbf{R}^{\text{MH}}) \geq \lambda_\eta(\mathbf{R})$ ,  $\eta = 1, 2, 3$ , i.e., the approximate eigenvalues of the coarse-scale resistivity tensor are upper bounds.

*Bilateral error bounds.* Above, upper bounds have been derived for

- (i) the coarse-scale permeability tensor  $\mathbf{K}$  defined as a ‘pressure-dissipation average’ in combination with the conformal-nodal finite element method, and
- (ii) the coarse-scale resistivity tensor  $\mathbf{R}$  defined as a ‘flux-dissipation average’ in combination with the mixed-hybrid finite element method.

It can be proved that, for *periodic* media, pressure-dissipation averaging and flux-dissipation averaging yield the same result  $\mathbf{K} = \mathbf{R}^{-1}$  [31]. This is also consistent with equations (3.i), (3.ii) and (7.i), (7.ii). Hence,  $\lambda_\eta(\mathbf{R}) = \Lambda_{3-\eta+1}^{-1}$ , and defining  $\Lambda_\eta^{\text{MH}} = \lambda_{3-\eta+1}^{-1}(\mathbf{R}^{\text{MH}})$ , it follows that

$$\Lambda_\eta^{\text{MH}} \leq \Lambda_\eta \leq \Lambda_\eta^{\text{CN}}, \quad \eta = 1, 2, 3. \quad (16)$$

This condition can be used to confine the unknown exact solution between upper and lower error bounds as they come closer together when refining the finite element grid.

Finally, it is remarked that the block-centered finite difference method, which is highly popular in reservoir engineering, is equivalent with a form of mixed hybrid finite elements [1,29], which explains the lower bound properties of this method [24].

## 6. Numerical examples using conformal-nodal and mixed-hybrid finite elements

Software based on the conformal nodal and the mixed hybrid finite element method has been developed. The software is coded in portable standard FORTRAN-77 and can be used both ‘stand alone’ (on workstations and PCs) and as callable subroutines in reservoir simulators.

**Numerical example 2** (No preferential flow paths). Let us consider the example presented in figure 6. The highly permeable regions have a permeability of 100 mD, while the low-permeability surroundings have a permeability of 1 mD. In this case there are no preferential flow paths. Note that we have the same number of highly permeable cells as in the example with preferential flow paths (figure 1). Due to the absence of preferential flow paths, it is obvious that in this case the effective permeability will be much lower.

Again using a mesh with  $N_a = 20 \times 12 \times 30 = 7200$  active nodes, the solution is

$$K_{ij} = \begin{pmatrix} 3.319 & 0 & 0.2939 \\ 0 & 42.25 & 0 \\ 0.2939 & 0 & 2.442 \end{pmatrix} \text{ mD}, \quad K_{\eta\mu} = \begin{pmatrix} 3.409 & 0 & 0 \\ 0 & 42.25 & 0 \\ 0 & 0 & 2.352 \end{pmatrix} \text{ mD},$$

with the angle equal to  $16.91^\circ$ .

**Numerical example 3** (Heterogeneity in all directions). In the following example (figure 9) the permeability has been made heterogeneous in the  $y$  direction. The highly permeable regions have now been made heterogeneous by redefining  $k(y) = 100\{1 -$

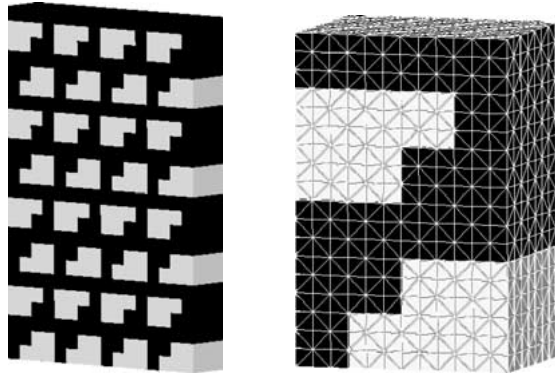
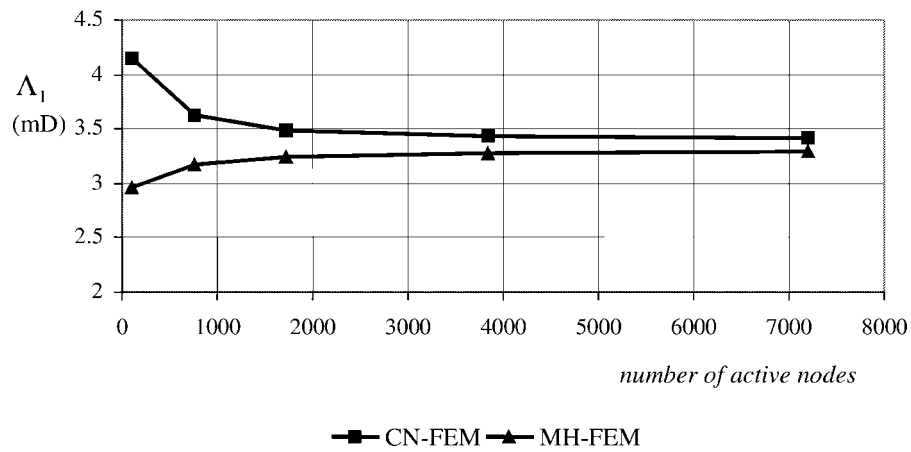
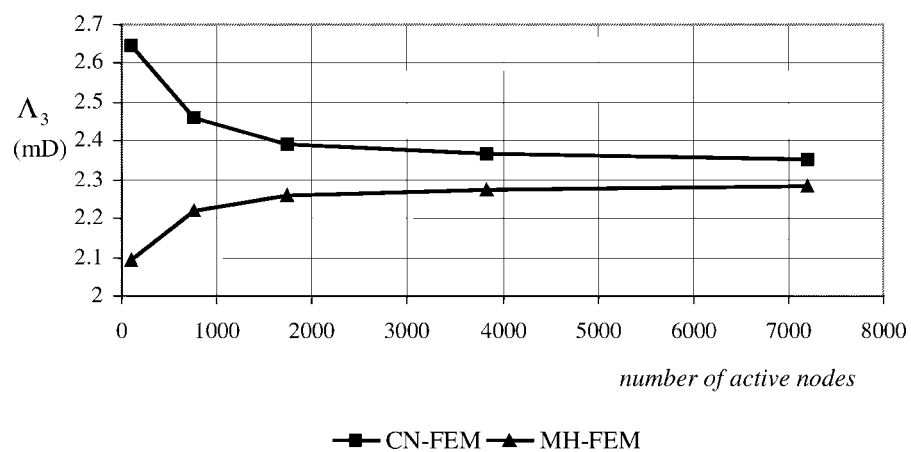


Figure 6. Example without preferential flow paths.

Figure 7. Eigenvalue  $\Lambda_1$  of coarse-scale permeability.Figure 8. Eigenvalue  $\Lambda_3$  of coarse-scale permeability.

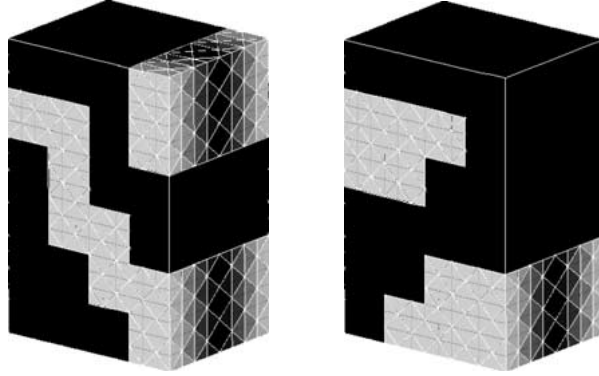


Figure 9. Example with and without preferential flow paths, with variations in the  $y$  direction.

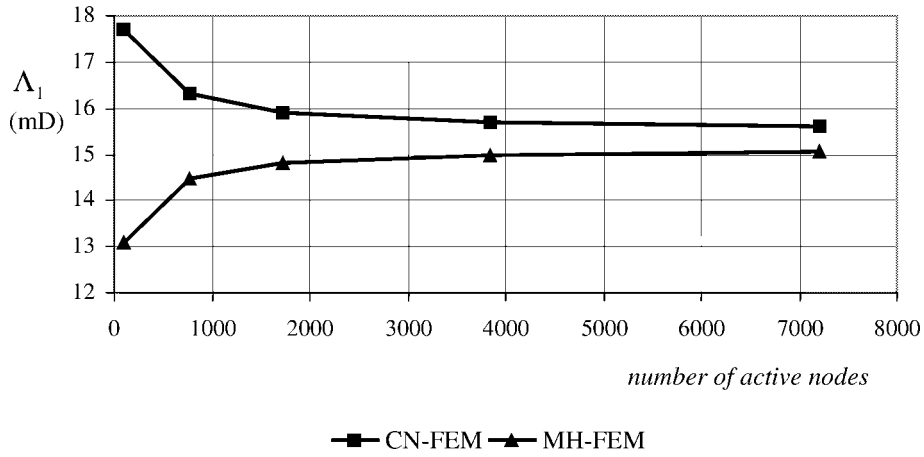


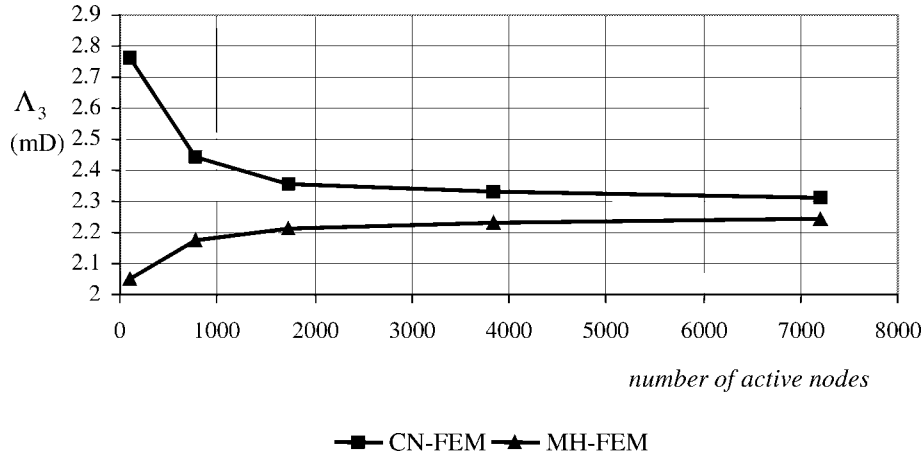
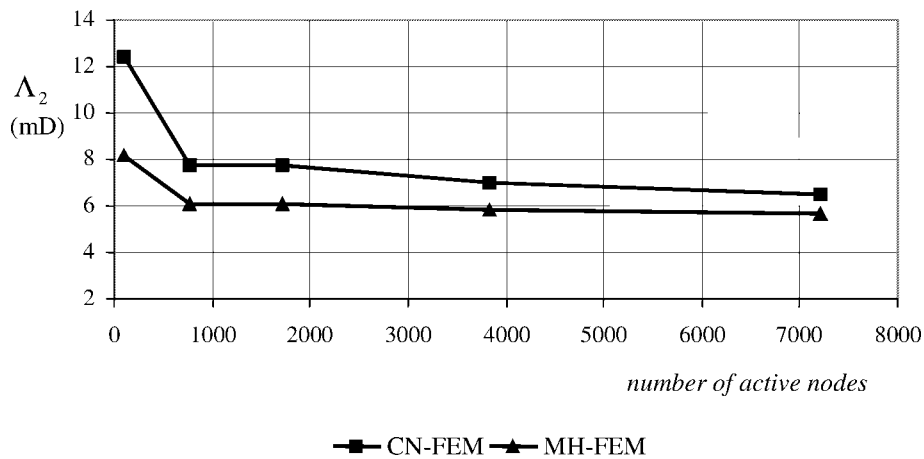
Figure 10. Eigenvalue  $\Lambda_1$  of coarse-scale permeability.

$(1 - 10^{-2}) \sin^2 5y$  mD. The thus-defined permeability varies periodically from 100 to 1 mD in the interval  $0 \leq y < 2\pi$ . Two permeability patterns: with and without preferential flow paths are considered.

Computations performed with the conformal-nodal finite element method on a mesh consisting of the same number of nodes as before, yield for the two cases respectively

$$K_{ij} = \begin{pmatrix} 6.330 & 0 & -6.106 \\ 0 & 6.474 & 0 \\ -6.106 & 0 & 11.59 \end{pmatrix} \text{ mD}, \quad K_{ij} = \begin{pmatrix} 3.092 & 0 & 0.257 \\ 0 & 6.516 & 0 \\ 0.257 & 0 & 2.328 \end{pmatrix} \text{ mD},$$

where the rotation angles are respectively equal to  $-56.65^\circ$  and  $16.93^\circ$ .

Figure 11. Eigenvalue  $\Lambda_3$  of coarse-scale permeability.Figure 12. Eigenvalue  $\Lambda_2$  of coarse-scale permeability.

The results obtained for the two heterogeneity patterns in the principal coordinate system are as follows:

$$K_{\eta\mu} = \begin{pmatrix} 15.61 & 0 & 0 \\ 0 & 6.474 & 0 \\ 0 & 0 & 2.313 \end{pmatrix} \text{ mD}, \quad K_{\eta\mu} = \begin{pmatrix} 3.170 & 0 & 0 \\ 0 & 6.516 & 0 \\ 0 & 0 & 2.250 \end{pmatrix} \text{ mD}.$$

As before, more meaningful information can be derived while comparing the solutions obtained with the two numerical methods; this is presented for the example with preferential flow paths (figures 10–12). At first glance, it seems that lower and upper bound rules are violated as far as values in  $y$  direction are considered (figure 12). However, this apparent violation is due to the fact that the fine-scale permeability is given as a continuous function of  $y$ . Since, in the finite element methods developed here, the

permeabilities are taken constant in each tetrahedral element, the discrete problems defined on different meshes are *different*. The constant value has been chosen equal to the permeability's value in the barycenter of the tetrahedron.

## 7. Upscaling around a well

The above-presented approach to upscaling will now be extended to upscaling around a well. For that purpose, a circular cylindrical homogenization cell around the well is transformed to an equivalent rectangular volume by the introduction of circular cylinder coordinates  $r, \varphi, z$ .

Writing the equations in  $r, \varphi, z$  coordinates, we end up with equations having the same form as (1) and (6), but now the interpretation of the coordinates is  $x = r, y = \varphi$ . In addition, multiplication or division with the metrical coefficient  $r = x$  transforms the permeability components. Homogenization of this transformed fine-scale permeability can be accomplished in the conventional way and yields a transformed coarse-scale permeability. The back transformation is based on finding the homogeneous fine-scale permeability (see the lower circle of figure 13) that yields the same transformed coarse-scale permeability as the original heterogeneous fine-scale permeability (see the upper circle of figure 13). This homogeneous permeability is then considered as the coarse-scale permeability around the well [32].

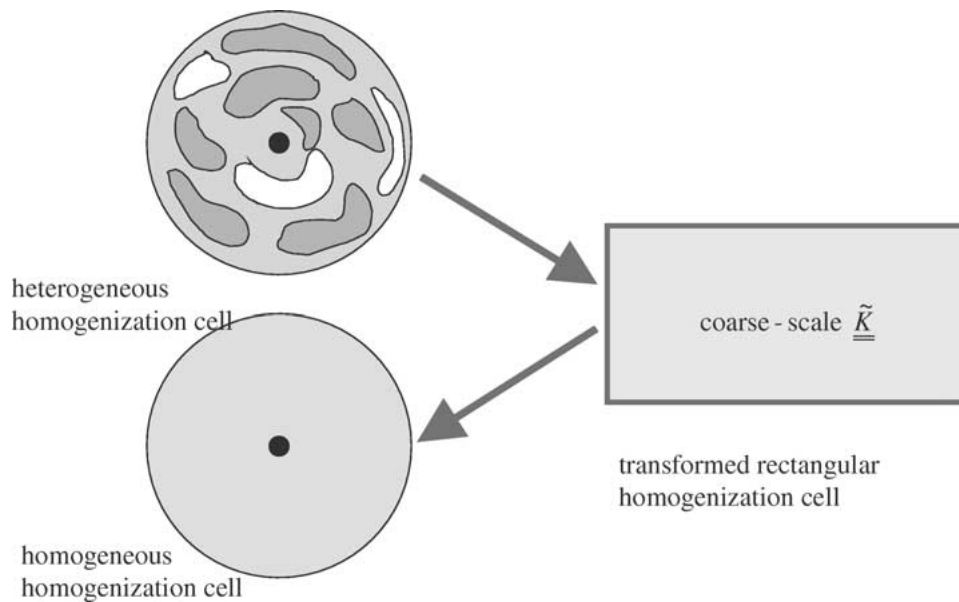


Figure 13. Transformation of circular upscaling cell for heterogeneous medium (upper circle) to rectangular homogenization cell and back transform to circular upscaling cell for equivalent homogeneous medium (lower circle).

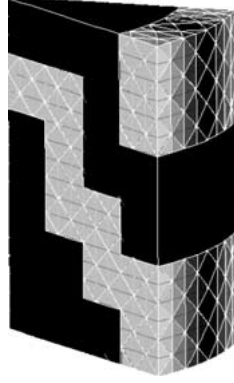


Figure 14. Segment with preferential flow paths around a vertical well; black blocks correspond with 1 mD; in grey cells  $k$  varies as function of  $\varphi$ .

**Numerical example 4** (Preferential flow paths). A circular geological structure with a vertical well in its center has an isotropic absolute permeability of 1 mD. This structure is cut by highly permeable faults with a permeability  $k(\varphi) = 100\{1 - (1 - 10^{-2}) \sin^2 5\varphi\}$  mD. In the  $(r, z)$ -planes  $\varphi = (1 + 2n)\pi/10$  the permeability is homogeneous and equal to 1 mD.

A segment  $\Delta r = 0.8$  m,  $\Delta\varphi = \pi/5$  and  $\Delta z = 1.2$  m represents a periodicity cell with radius  $a = 0.05$  m (figure 14). One, or more periodicity volumes may be considered as the ‘natural’ choice of a homogenization cell. Since the transformed permeabilities are  $\tilde{k}_{rr} = \tilde{k}_{zz} = rk$  and  $\tilde{k}_{\varphi\varphi} = k/r$ , there is only approximate periodicity of  $\tilde{k}_{ij}$  in the  $r$  direction. Nevertheless the equations are solved with periodic boundary conditions.

Using a mesh with  $N_a = 20 \times 12 \times 30$  active nodes, homogenization based on the conformal-nodal finite element approximation yields

$$K_{ij} = \begin{pmatrix} 7.315 & 0 & -7.521 \\ 0 & 5.152 & 0 \\ -7.521 & 0 & 13.63 \end{pmatrix} \text{ mD}, \quad K_{\eta\mu} = \begin{pmatrix} 18.63 & 0 & 0 \\ 0 & 5.152 & 0 \\ 0 & 0 & 2.317 \end{pmatrix} \text{ mD},$$

where the rotation angle is  $-56.39^\circ$ .

Using the same mesh, the approximate solution of this homogenization problem obtained by the mixed-hybrid finite element method is

$$K_{ij} = \begin{pmatrix} 7.053 & 0 & -7.281 \\ 0 & 5.152 & 0 \\ -7.281 & 0 & 13.075 \end{pmatrix} \text{ mD}, \quad K_{\eta\mu} = \begin{pmatrix} 17.94 & 0 & 0 \\ 0 & 5.152 & 0 \\ 0 & 0 & 2.185 \end{pmatrix} \text{ mD},$$

where the rotation angle is  $-56.23^\circ$ .

**Numerical example 5** (No preferential flow paths). A cylindrical homogenization cell  $\Delta r \times \Delta\varphi \times \Delta z = 0.8 \text{ m} \times \pi/5 \times 1.2 \text{ m}$  around a well with radius is  $a = 0.05 \text{ m}$

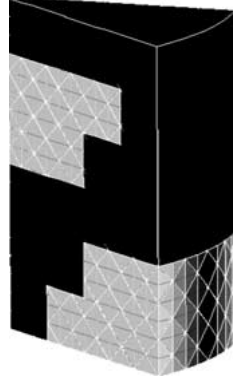


Figure 15. Segment without preferential flow paths around a vertical well.

is considered figure 15. This time there are no preferential flow paths within the cell. Homogenization based on the conformal-nodal finite element approximation yields

$$K_{ij} = \begin{pmatrix} 4.412 & 0 & 0.367 \\ 0 & 6.192 & 0 \\ 0.367 & 0 & 2.361 \end{pmatrix} \text{ mD}, \quad K_{\eta\mu} = \begin{pmatrix} 4.476 & 0 & 0 \\ 0 & 6.192 & 0 \\ 0 & 0 & 2.298 \end{pmatrix} \text{ mD},$$

where the rotation angle is  $9.85^\circ$ .

The approximate solution to the same homogenization problem with the mixed-hybrid finite element method is

$$K_{ij} = \begin{pmatrix} 3.958 & 0 & 0.352 \\ 0 & 5.113 & 0 \\ 0.352 & 0 & 2.223 \end{pmatrix} \text{ mD}, \quad K_{\eta\mu} = \begin{pmatrix} 4.027 & 0 & 0 \\ 0 & 5.113 & 0 \\ 0 & 0 & 2.154 \end{pmatrix} \text{ mD},$$

where the rotation angle is  $11.04^\circ$ .

*Global upscaling – validation.* To check the correctness of homogenization under circumstances where there is no exact periodicity, global upscaling is performed. Global upscaling uses the same homogenization cell. However, now the modeling domain has been ‘blown up’ to much larger size. In this example the flow is modeled in the region  $\Delta r \times \Delta \varphi \times \Delta z = 9.6 \text{ m} \times \pi/5 \times 1.2 \text{ m}$  on which the orthonormal periodic boundary conditions are specified. In this case, equations (3.i), (3.ii), or respectively (7.i), (7.ii) do no longer hold. Instead, the ‘pressure-flux’ (PF) approach based on the coarse-scale Darcy’s law  $\langle \mathbf{q}_i \rangle = \mathbf{K}^{\text{PF}} \cdot \langle \text{grad } p_i \rangle$  is used to find the coarse-scale permeability  $\mathbf{K}^{\text{PF}}$ , while also the ‘pressure-dissipation’ (PD) approach based on the coarse-scale dissipation equation  $\langle \text{grad } p_i \rangle \cdot \mathbf{K}^{\text{PD}} \cdot \langle \text{grad } p_j \rangle = \langle \text{grad } p_i \cdot \mathbf{k} \cdot \text{grad } p_j \rangle$  is used to find the coarse-scale permeability  $\mathbf{K}^{\text{PD}}$ . Then the nine individual coarse-scale components have to be computed from a system of nine linear equations.

Pressure-dissipation averaging yields

$$K_{ij}^{\text{PD}} = \begin{pmatrix} 7.521 & 0 & -8.261 \\ 0 & 5.033 & 0 \\ -8.261 & 0 & 14.46 \end{pmatrix} \text{ mD}, \quad K_{\eta\mu}^{\text{PD}} = \begin{pmatrix} 19.95 & 0 & 0 \\ 0 & 5.033 & 0 \\ 0 & 0 & 2.031 \end{pmatrix} \text{ mD},$$

where the rotation angle is  $-56.39^\circ$ . Pressure-flux averaging yields an a-symmetric transformed permeability  $\tilde{K}_{ij}$ . However, since virtually all reservoir simulators require a symmetric homogenized mobility  $K_{ij}$  as input parameter, the back transformation has been based on the symmetric part  $(\tilde{K}_{ij} + \tilde{K}_{ji})/2$ , yielding a symmetric coarse-scale permeability

$$K_{ij}^{\text{PF}} = \begin{pmatrix} 7.813 & 0 & -8.027 \\ 0 & 5.158 & 0 \\ -8.027 & 0 & 15.33 \end{pmatrix} \text{ mD}, \quad K_{\eta\mu}^{\text{PF}} = \begin{pmatrix} 20.44 & 0 & 0 \\ 0 & 5.158 & 0 \\ 0 & 0 & 2.708 \end{pmatrix} \text{ mD},$$

where the rotation angle is  $-57.55^\circ$ . Again, the mesh with  $N_a = 20 \times 12 \times 30$  active nodes has been used.

Comparing the thus obtained results with the results from sections 4 and 6 shows that homogenization around a well may be considered as a reasonable approximation. If more accuracy is required, global upscaling might be the right action. Doing so there is some vagueness in what exactly is meant by ‘upscaling,’ since pressure-flux averaging, pressure-dissipation averaging and flux-dissipation averaging may yield three different results.

## 8. Summary and conclusions

To numerically determine equivalent homogeneous permeabilities at a coarse-scale level from a spatially oscillating fine-scale permeability distribution, two complementary types of finite element methods have been used. First it is shown that, if the porous medium is periodic, the upscaling can be performed by the homogenization method. If there are deviations from periodicity, for instance in the form of trends superimposed on the periodicity, global upscaling approaches might be a more appropriate alternative. However, it is shown that there are at least two equally justifiable global methods, yielding two different coarse-scale permeabilities. Since these differences disappear for periodic media, homogenization is still an acceptable alternative, even for a-periodic media.

Numerical homogenization gives rise to an approximation error. To quantify this error, the computations are performed twice, using two complementary numerical methods: the conformal-nodal finite element method and the mixed-hybrid finite element method. It is proved and exemplified that these two methods yield respectively upper and lower bounds for the eigenvalues of the coarse-scale permeability. Convergence to the exact solution can then be obtained by global and local mesh refinement. Results of numerical experiments obtained using 3D tetrahedral-based finite element codes are shown, both in the far field and around wells.

## Acknowledgements

This work has partly been sponsored by Norsk Hydro, Reserch Center Bergen, Norway. The inspiring discussions with Ivar Aavatsmark (Norsk Hydro) are gratefully acknowledged.

## References

- [1] T. Arbogast, M.F. Wheeler and I. Yotov, Mixed finite elements for elliptic problems with tensor coefficients as cell-centered finite differences, *SIAM J. Numer. Anal.* 34(2) (1997) 828–852.
- [2] D.N. Arnold and F. Brezzi, Mixed and nonconforming finite element methods: Implementation, post-processing and error estimates, *RAIRO Modél. Math. Anal. Numér.* 19 (1985) 7–32.
- [3] J.-L. Auriault, Effective macroscopic description for heat conduction in periodic composites, *Internat. J. Heat Mass Transfer* 26(6) (1983) 861–869.
- [4] J. Bear, *Dynamics of Fluids in Porous Media* (Dover, New York, 1972).
- [5] A. Bensoussan, J.-L. Lions and G. Papanicolaou, *Asymptotic Analysis for Periodic Structures* (North-Holland, Amsterdam, 1978).
- [6] A. Bossavit, *Computational Electromagnetism* (Academic Press, San Diego, 1998).
- [7] F. Brezzi and M. Fortin, *Mixed and Hybrid Finite Element Methods* (Springer, New York, 1991).
- [8] H.S. Carslaw and J.C. Jaeger, *Conduction of Heat in Solids* (Oxford Univ. Press, Oxford, 1959).
- [9] C.M. Case, *Physical Principles of Flow in Unsaturated Porous Media* (Oxford Univ. Press, New York, 1994).
- [10] F. Chatelin, *Spectral Approximation of Linear Operators* (Academic Press, New York, 1983).
- [11] J. Douglas, Jr., M. Peszyńska and R.E. Showalter, Single phase flow in partially fissured media, *Transport Porous Media* 28 (1997) 285–306.
- [12] M.E. Gurtin, Variational principles for linear initial value problems, *Quart. Appl. Math.* 22(3) (1964) 252–256.
- [13] U. Hornung, *Homogenization and Porous Media* (Springer, Berlin, 1997).
- [14] E.F. Kaasschieter, Preconditioned conjugate gradients for solving singular systems, *J. Comput. Appl. Math.* 24 (1988) 265–275.
- [15] E.F. Kaasschieter and A.J.M. Huijben, Mixed-hybrid finite elements and streamline computations for the potential flow problem, *Numer. Methods Partial Differential Equations* 8 (1992) 221–226.
- [16] P.R. King, The use of renormalization for calculating effective permeability, *Transport Porous Media* 4 (1987) 37–58.
- [17] C. Lanczos, *The Variational Principles of Mechanics* (Dover, New York, 1970).
- [18] J.A. Meijerink and H.A. Van der Vorst, An iterative solution method for linear systems of which the coefficient matrix is a symmetric M-matrix, *Math. Comp.* 31 (1977) 148–162.
- [19] Ph.M. Morse and H. Feshbach, *Methods of Theoretical Physics* (McGraw-Hill, New York, 1953).
- [20] J.C. Nédélec, Mixed finite elements in  $\mathbf{R}^3$ , *Numer. Math.* 35 (1980) 315–341.
- [21] M. Panfilov, *Macroscale Models of Flow Through Heterogeneous Porous Media* (Kluwer Academic, Dordrecht, 2000).
- [22] M. Peszyńska, On a model of nonisothermal flow through fissured media, *Differential and Integral Equations* 8(6) (1995) 1497–516.
- [23] R.A. Raviart and J.M. Thomas, A mixed finite element method for 2nd order elliptic problems, in: *Mathematical Aspects of the Finite Element Method*, Lecture Notes in Mathematics, Vol. 606 (Springer, New York, 1977) pp. 292–315.
- [24] R.F. Ribeiro and R.K Romeu, Computing the effective permeability by finite differences, finite elements, and mixed-hybrid finite elements (1997).

- [25] E. Sanchez-Palencia, Non-homogeneous media and vibration theory, in: *Lecture Notes in Physics*, Vol. 127 (Springer, Berlin, 1980).
- [26] G. Strang and G.J. Fix, *An Analysis of the Finite Element Method* (Prentice-Hall, Englewood Cliffs, NJ, 1973).
- [27] A. Trykozko, Analyse de quelques méthodes de maillage adaptif, Électricité de France, Document HI-72/7715, Clamart, France (1991).
- [28] A. Weinstein and W. Stenger, *Methods of Intermediate Problems for Eigenvalues* (Academic Press, New York, 1972).
- [29] A. Weiser and M.F. Wheeler, On convergence of block-centered finite-differences for elliptic problems, *SIAM J. Numer. Anal.* 25 (1988) 351–375.
- [30] W. Zijl and M. Nawalany, *Natural Groundwater Flow* (CRC/Lewis, Boca Raton, FL, 1993).
- [31] W. Zijl and A. Trykozko, Numerical homogenization of the absolute permeability using the conformal-nodal and the mixed-hybrid finite element method, *Transport Porous Media* (2001) in press.
- [32] W. Zijl and A. Trykozko, Numerical homogenization of the absolute permeability tensor around wells (2001) submitted.